

Metallic Nanobrushes Made using Ambient Droplet Sprays

Depanjan Sarkar, Maheswari Kavirajan Mahitha, Anirban Som, Anyin Li, Michael Wleklinski, Robert Graham Cooks,* and Thalappil Pradeep*

There are important implications for science and technology in the ability to create structures composed of tens of micrometer long, uniformly aligned, nanowires. They include improvements in understanding electronic structures of materials, creation of photonic devices, band gap engineering, and surface-derivatized nanostructures for use as sensors and for fundamental studies of catalysis.^[1] While advances in materials science have contributed various methods for the synthesis of aligned nanostructures on surfaces, often such methods involve processing in vacuum and/or the use of special features like magnetic fields,^[2] dipole–dipole attraction,^[3] directional freezing,^[4] and template mediation.^[5] Here, we introduce an ambient solution-state procedure for making oriented 1D nanostructures which can cover and pattern large areas.

Spray pyrolysis is an established method of making materials,^[6] especially thin films. Several variations of this method exist which result in nanoscale oxides^[7] and related materials. However, these methods do not produce metal nanoparticles. Anisotropic growth of nanostructures has not been observed in such cases. Here we report spontaneous electric field induced assembly of charged microdroplets in air, producing nanowires (NWs) by the 1D assembly of nanoparticles (NPs). The possibility of extending this over cm^2 areas and control of individual wires so prepared are presented here. The possibility to control compositions and novel properties of the structures derived are demonstrated.

In the present experiment, a home-built nanoelectrospray source was directed to deliver charged droplets of silver acetate (AgOAc) in water onto a conductive mesh (usually a transmission electron microscopy (TEM) grid), placed on top of an indium tin oxide (ITO) coated glass collector. The TEM grid was used as a static mask to intercept a portion of the spray plume. The collector was grounded through a picoammeter to monitor the deposition current and a potential in the range of 1–1.5 kV was applied to the solution through a platinum (Pt) wire electrode. A plume of solvated silver ions (notably, $\text{Ag}(\text{H}_2\text{O})^+$ and $\text{Ag}(\text{H}_2\text{O})_2^+$) was ejected from the nanospray tip, as confirmed

by mass spectrometry. Figure 1A,C shows an optical image of the sprayer, the spray plume, and the mass spectrum collected from the plume, respectively.

In the course of silver deposition, a black circular spot (typical diameter 2 mm) due to the impinging plume appeared on the mask itself. Microscopy of the grid revealed an unprecedented brush-like growth of nanowires, with a linear arrangement of NPs comprising each nanowire. Figure 1B,D shows TEM images of such nanowires at different magnifications. A higher magnification image of the same sample (Figure 1D) clearly shows a structure having linear morphology, some of them somewhat bent. The growth in each NW is clearly 1D and not dendritic; although the imaging electron beam can cause the wires to adhere (Figures 1C, 2A); they are clearly not branched. This 1D wire-like growth occurred only on the mask: the same ion plume generated a collection of NPs when it fell directly onto the collector (Figure S1, Supporting Information). Close examination showed that the NWs are typically assembled in small groups (nanobristles) and these in turn are arrayed on the surface to create a nanobrush. Each nanobristle is braided. Figure 1D shows a TEM image from the tip of a brush, where it is clear that nanobristles are protruding from the brush. So, this image proves that each brush is a braid of a member of nanowires of 5–7 nm diameter. If we look closely at the nanobristles, they are composed of NPs of similar shape and size, oriented linearly (Figure 1E), reminiscent of the conidial growth of fungi. In short, deposition of the solvated metal ion plume results in neutralization, aggregation, and orientation to form nanostructures.

Detailed examination of the TEM data reveals further interesting features. A TEM image of a single square of the mesh (Figure 2A) shows uniform arrays of bristles of NW structures protruding from the vertical edges of the grid. The apparently continuous nanowires and nanobristles in low magnification (Figures 1B and 2A) images prove, upon closer inspection, to have a “pearl necklace” morphology, derived from individual nanoparticles (Figures 1E and 2B inset). The TEM image in Figure 2B inset shows the assembly of NPs leading to elongated NW growth and their assembly into bristles. In this experiment, the wire length was kept deliberately small by controlling the deposition time, to reduce electron beam induced distortions of the individual structures. Figure S2 in the Supporting Information shows TEM images of such an aggregated structure where individual NPs of similar sizes are clearly visible. Figure 2B shows a high resolution transmission electron microscopy (HRTEM) image of one of the NPs in a nanowire. The measured Ag (111) lattice spacing (Figure 2B) and scanning electron microscopic–energy dispersive spectroscopy (SEM–EDS) spectrum (Figure S3, Supporting Information), confirm the presence of crystalline AgNPs.

D. Sarkar, M. K. Mahitha, A. Som, Prof. R. G. Cooks, Prof. T. Pradeep
DST Unit of Nanoscience (DST UNS) and
Thematic Unit of Excellence (TUE)
Department of Chemistry
Indian Institute of Technology Madras
Chennai 60036, India
E-mail: cooks@purdue.edu; pradeep@iitm.ac.in

Dr. A. Li, M. Wleklinski, Prof. R. G. Cooks, Prof. T. Pradeep
Department of Chemistry
Purdue University
West Lafayette, IN 47907, USA

DOI: 10.1002/adma.201505127



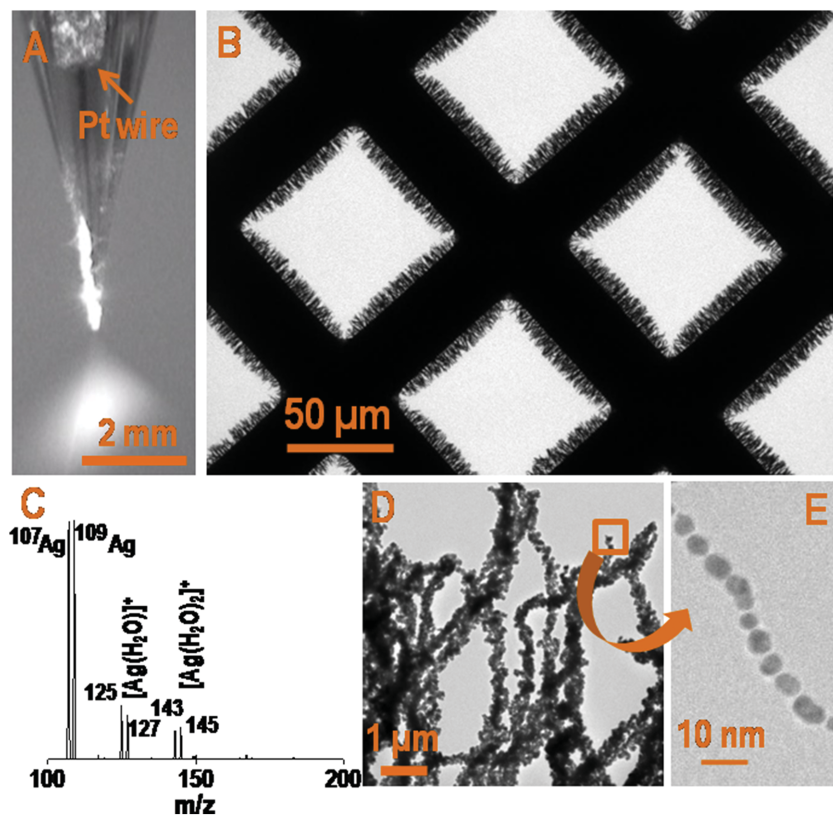


Figure 1. A) Optical image of an electro spray experiment using AgOAc solution, showing the spray plume, B) large area TEM image of an empty TEM grid (used as mask during deposition) showing uniform NWs all over it, C) mass spectrum collected from the spray showing the presence of Ag and solvated Ag ions, D) TEM image of the nanobrush formed on the mask (an empty TEM grid in this case), showing 1D structure of the NWs, and E) Higher magnification TEM image of single building block (NW) with its pearl necklace morphology.

TEM images are 2D projections of 3D objects; hence they may be misinterpreted to imply that the NW structures are formed only at the edges of the square apertures of the mesh. For better understanding of their growth, field emission scanning electron microscopic (FESEM) analysis was performed on the circular plume spot ($\approx 1.5\text{--}2.5$ mm in diameter, depending upon the distance of the collector surface from the spray emitter) on the mask. An FESEM image (Figure 2C) of the grid surface shows uniform growth of nanostructures all over the exposed surface of the grid, not only at its edges. A magnified image (Figure 2D) shows that the growth of the metallic brush appears as an extended grassland-like morphology.

The images just discussed were typically of those collected from a sample that had undergone electro spray (1 mM AgOAc solution) for 1 h. Typical deposition currents during electro spray were 40 nA corresponding to an arrival rate of 2×10^{12} ions s^{-1} . On a 2 mm diameter spot, this converts to ≈ 213 monolayers (ML) in 1 h. Using the Ag lattice constant of 0.408 nm, the thickness of 213 contiguous silver layers (of (110) stacking) is about 86.5 nm. The actual measured length of the NWs in a typical experiment is 20 micrometer, ≈ 231 times greater. The major source of this difference is the sparse spacing of the NWs making up the nanobrush surface. Figure 2A shows that in a linear distance of 100 micrometer, only about

50 nanobristles (≈ 60 nm each, composed of ≈ 75 NWs) exist. This $\approx 0.3\%$ occupancy of the available space gives rise to the ≈ 3 orders of magnitude increase in the number of layers of Ag found in the NW forming regions. The NW growth occurs only when the droplets were neutralized on the conducting grid. Powerful organizing forces must be involved in such dramatic structuring of a surface to create these brush structures. Obviously NPs formed by the deposition are arranged by this organization force, as evident from the 1D assembly shown in Figure 1E.

Coulombic assembly and basic mechanism: Aspects of the mechanism of NW growth are the following. First, as just noted, powerful electrostatic forces are involved. Second, the crystalline nature of the NWs suggests that microdroplets or solvated metal ions are deposited on the surfaces and spatial reorganization occurs while solvent is evaporating leaving behind a neutralized silver deposit. Third, small NP “pearls” attach to each other to form the growing nanowire. The edges of these structures are rough, which is ascribed to head-on accumulation of NPs as well as their orthogonal association to form nanobristles. Finally, the NPs constituting the NWs are remarkably uniform in size, especially considering that no capping agent is used. These facts are all consistent with a Coulombic control mechanism. The electric field strength near the wires which form on the grounded metal grid is strongly enhanced with field lines radiating out from these structures. The Coulombic force due to the potential difference (≈ 1200 V, and the field strength calculated at this potential difference was 2×10^5 V m^{-1}) between the grid and the emitter harpoons metal ion microdroplets into the high field region and deposits and neutralizes them on the metal grid surface. At high fields, especially after some NW growth, field emission may be important in determining droplet neutralization. The material so formed represents a point of even higher electric field and this leads to the growth of elongated NWs. The fact that lengths of the NWs are attenuated (clearly visible in Figure 2A) in the corners of the grid also supports the role of electric fields in the growth of NWs because of the lower electric fields there. We do not understand why the NPs which make up the NWs have well-defined (5–7 nm) sizes. It could be because each microdroplet contains approximately the same number of Ag ions as there are in a 5–7 nm particle. A deposition current of 40 nA and solvent flow rate of 20 nL min^{-1} would contain enough silver ions to produce 5–7 nm NPs if the droplets were 260–370 nm in size. Droplets smaller than 500 nm cannot be visualized but have been estimated^[8] as a plausible size in nanoelectrospray ionization. In this mechanism, the next incoming droplet would drop its cargo of Ag making a new NP instead of aggregating with the previous NP. The growth of 1D NWs would be due to preferred

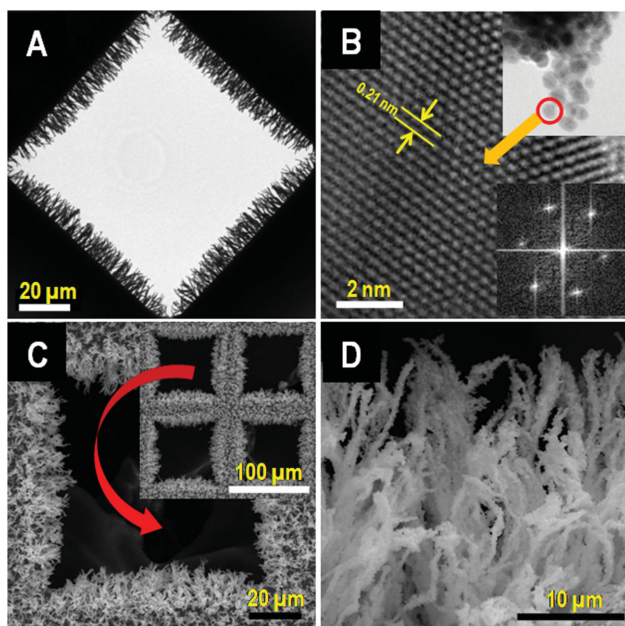


Figure 2. A,B) TEM images; C, D) FESEM images. A) TEM image of a grid after electro spray deposition of Ag, B) HRTEM shows Ag lattice plane in one NP constituting the brush, inset is a high magnification TEM image showing a “pearl necklace” collection of NPs, C) FESEM of the same grid showing Ag growth all over the grid (inset shows large area image), and D) high magnification SEM image of the same grid showing rough edges of the NWs.

deposition at a NW tip (or nascent NW tip), as a result of the enhanced high electric field that exists at the tips of the NWs.^[9] A difficulty with this mechanism is the lack of experimental evidence that the NW geometry depends on spray distance and hence droplet size and the fact that a relatively tight range of droplets sizes must be invoked. Note that the process could continue to extend NWs until very long structures have been grown as shown in Figure 2D and in Figure S4 in the Supporting Information, where an aperture in the grid is almost closed by the inwardly growing NWs. A control experiment demonstrated the role of the electric field in the formation of both the NPs collected on the ITO substrate and the NWs collected on the mask. In this experiment, one TEM grid was laid on top of another with in-plane rotation to avoid complete superimposition so that a portion of the bottom grid is exposed to the impinging ion beam. Deposition of silver ions now gives SEM images (Figure S5, Supporting Information) which demonstrate that the bottom grid did not grow brushes, it only accumulated AgNPs, just as the ITO slide did; on the other hand, brushes formed on the top grid. This experiment was repeated with different concentration of solution. The result obtained in all the cases were same as discussed above. We interpret this result as suggesting that the cavity formed by the grid above the open spots on the bottom surface acts to weaken the electric field at this surface and that a strong electric field is responsible for creating the strong Coulombic force which causes charged microdroplets to be deposited as NWs.

Rapid deposition, use of other substrates and applications: The low dose of silver in these deposition experiment means that it takes a long time to make long wires or large area structures,

so higher flux experiments were performed using higher concentrations of silver salts. Interestingly the structures were unaffected by the increasing concentrations. The TEM images (Figure S6, Supporting Information) show that longer structures were produced using higher concentration in much less time. Figure S6 in the Supporting Information shows TEM images of this growth using electro spray deposition of 10 mM solution. Figure S6A,B in the Supporting Information shows the growth after 3 and 5 h spray time, respectively. In all the above experiments, copper grids were used as masks for NW deposition, but other mask materials like stainless steel (SS) wire mesh were also used. Figure S7 in the Supporting Information shows similar growth of silver on the SS wire mesh. Metallic or in general, conducting mesh surfaces, appear to be necessary for the growth of nanobrushes. Insulating surfaces do not grow brushes. Figure S7C,D shows SEM images of Ag deposition on cotton cloth. In this case no 1D NWs were seen. Hence we propose that a conducting metallic mesh is required for making these brushes. On the other hand, different underlying substrates gave the same result. Experiments were done with ITO-coated glass slide, copper plate, SS plate, etc. all of them accumulated AgNPs whereas the mesh on top formed NWs. Rapid deposition with morphology control may be important in applications.

Plasmonic nanostructures find use as sensors^[10] being surface enhanced Raman active substrates.^[11] Figure 3A shows a hyperspectral image of the AgNPs in the prepared nanobrush. The scattering spectra collected from these particles show sharp peaks, indicating that they are plasmonic, and have a small range of sizes. The inset (a) in Figure 3A shows a dark field optical image of Ag brushes protruding from the edge of a TEM grid. Continuous structures are not seen as they would have been broken by the coverslip which presses against them during imaging. Inset (b) in Figure 3A shows scattering spectrum collected from the AgNPs. The sharpness of the spectra proves that they are plasmonic in nature. X-ray photoelectron spectroscopic (XPS) analysis (Figure S8, Supporting Information) shows that the $3d_{5/2}$ peak of the brushes occur at 367.9 eV supporting the existence of Ag(0) state in the sample. Figure 3B shows a Raman image of a TEM grid, using 1×10^{-8} M crystal violet (CV) as the analyte. The copper edges of the grid are visible in the Raman image as they contain silver brushes which are SERS active. The inset shows the Raman spectrum of CV; an enhancement factor of 2.4×10^6 was measured.

The surface enhancement exhibited by these structures could be useful in sensing trace amounts of materials from air, automobile emissions or water as many of them have Raman spectral features. The advantages of these substrates in SERS are that the structures are readily made in air and can act like nanoscale brushes to capture particles or bacteria present in the air due to their mechanical porosity.

To demonstrate the capture of micron-sized particles, a mist of bacteria (from a suspension of *Escherichia coli*) was sprayed onto a NW structure, but the structures were easily destroyed by mechanical strain of the spray. To stabilize the structures, a molecular bond between the NPs was first established using 1,8-octanedithiol. After treatment with 1,8-octanedithiol, the brushes were strong enough to withstand a mechanical strain like an incoming spray plume from a commercial water spray

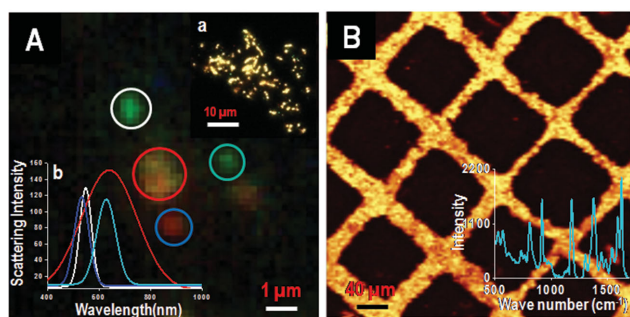


Figure 3. Hyperspectral images of the AgNPs. A) Inset a) shows a large area image, b) scattering spectra collected from AgNPs in a single NW, sharpness of the scattering spectrum taken from the particles shows that they are plasmonic in nature, each scattering spectrum is from an isolated particle or an aggregate (color variation is due to their size differences). Colors of the scattering spectra correspond to particles from which they were collected (with circles of the same color). B) Raman image of the Ag brush containing grid using 1×10^{-8} M crystal violet as analyte. Inset shows the corresponding Raman spectrum.

bottle. A pretreatment of the TEM grid was also performed with the same reagent to ensure strong bonding between the brush and the grid. The procedure of NP stabilization is elaborated in the methods section. This made the structures strong enough to be used as traps for particles in air flows. **Figure 4A,B** shows SEM images of *E. coli* captured by the brushes from a mist

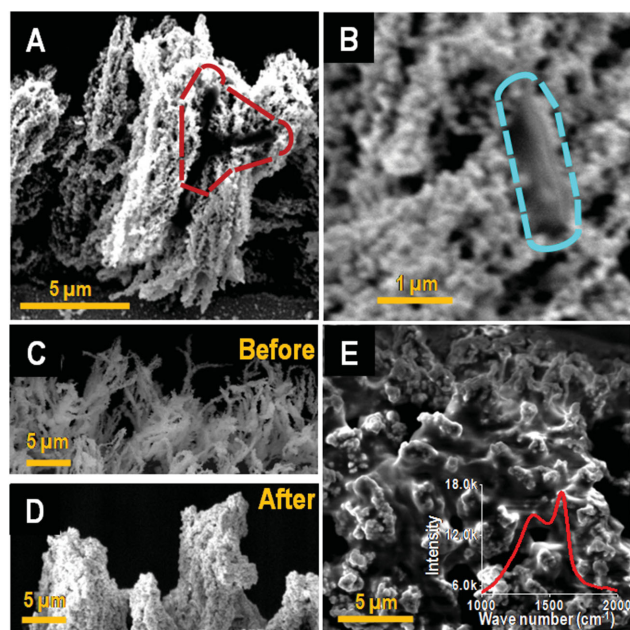


Figure 4. A, B) SEM images of the Ag brush on grid after capturing *E. coli* from corresponding suspensions. The dashed line, in (A) shows an area where *E. coli* is trapped among the brushes, and in (B) it shows the perimeter of a captured bacterium (without sputter coating of a metal film, the nonconductive bacteria show a vague image under SEM), C, D) SEM images of the brushes before and after 60 s exposure of $PM_{2.5}$, and E) SEM image of the brushes after 60 s exposure of $PM_{2.5}$, which was generated by burning incense sticks. Inset shows the Raman spectrum taken after $PM_{2.5}$ exposure; clear peak identifies black carbon present in this $PM_{2.5}$.

of bacterial suspension passing over it. As Ag is known to be antibacterial,^[12] the NWs are expected to kill captured bacteria. In the SEM image in Figure 4B one bacterial cell is visible, trapped in between the Ag brushes. Exploring additional applications, the brushes were shown to capture particulate matter ($PM_{2.5}$),^[13] when exposed to smoke created by burning incense which produced particles below 2.5 micron size. The SEM images (Figure 4C,D) show the brushes, before and after 60 s exposure to smoke. It is clear that they become thicker after capture. The SEM image shown in Figure 4E was taken after 300 s of exposure to smoke. The image clearly shows the presence of particulate matter in between the brushes also. Raman spectrum shown in the inset also supports the presence of carbonaceous material. SEM images in Figure S9 in the Supporting Information shows changes of Ag brushes with respect to time of smoke exposure. These brushes are not reusable; but can capture much more mass than their own body mass. This is possible due to the fact that they have substantial void space in between. The silver present in the material can be reused, however.

Composition control: Bimetallic brushes can be made by this methodology by changing the precursor composition. In an experiment, a 1:1 mixture of palladium acetate in acetonitrile (1 mM) and silver acetate in water (1 mM) was electrospayed and collected in the same way as described earlier (same as electrospay deposition of silver acetate). In this case also an empty TEM grid was used as a mask in between the spray tip and the collector surface. After deposition for 2 h at a deposition current of 45 nA, the mask was examined under an electron microscope. **Figure 5A–C** show SEM images, at different magnifications, of the grid showing the formation of thicker NWs than the earlier case (only Ag deposition). Figure 5D shows a SEM image of a single square of the TEM grid containing Ag brushes on it. Differences in morphology are clearly visible if we compare the images in Figures 5B,D. In the case of AgPd bimetallic structures, the NWs are not 1D in nature. TEM images (Figures 5E,F) taken from the same sample show the presence of crystalline AgPd NPs in each bristle. These brushes are made up of bimetallic NP assembly. Composition variation of Ag and Pd precursors has a significant role on the formation of bimetallic brushes. Control experiments show that when the content of Pd was high in the precursor solution (1:3 Ag/Pd), bimetallic brushes did not form.

Catalysis: These bimetallic structures can be used as catalytic platforms for different chemical reactions. **Figure 6** shows the mass spectrum of diphenylamine (DPA), polymerized using AgPd bimetallic brushes as a catalytic platform. In this experiment, first AgPd bimetallic structures were made on a stainless steel wire mesh and a 100 ppm methanolic solution of DPA was electrospayed at a deposition current of 40 nA for 10 min. After deposition of DPA, the brushes were washed gently with methanol and ESI mass spectrum of the solution was taken. It showed that DPA polymerizes on the AgPd bimetallic brushes. Conversion efficiency was calculated as 81% in the case of bimetallic brushes. To prove that these bimetallic brushes are playing a catalytic role in the polymerization reaction, control experiments were done. In one experiment the same solution of DPA was sprayed on an ITO-coated glass slide using the same deposition current

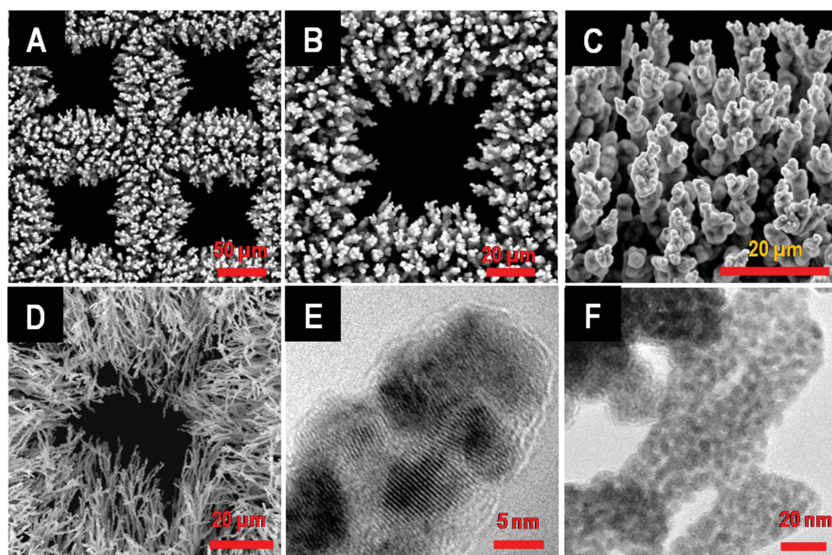


Figure 5. A–C) SEM images of AgPd bimetallic nanobrushes at different magnifications, D) SEM image of Ag brush showing different morphology in the case of bimetallic brushes, and E, F) TEM images of bimetallic structures showing the presence of AgPd NPs in each bristle.

(40 nA) as in the earlier case. After deposition was complete, the ITO-coated slide was washed with methanol and mass spectrum was taken. In this case polymerization was not seen, whereas a clear intense peak of DPA was visible in the spectrum at m/z 170 (Figure 6, inset). In another control experiment AgPd particles were deposited on a copper plate. We know that electro spray deposition of metal on copper does not produce any particular morphology: in this process NPs of the metal are deposited on the plate. In the control experiment, a 1:1 mixture of palladium acetate (1 mM) in acetonitrile and silver acetate (1 mM) in water was electro sprayed on the copper plate at the same deposition current (40 nA). The experiment was repeated with DPA on this bimetallic surface. The mass spectrum (Figure S10, Supporting Information) showed polymerization of DPA with a conversion efficiency of 58%. Although the amount of NPs deposited was more in this case because the whole spray plume was collected (there was no mask in this case), lower conversion efficiency was seen. This supports the fact that brush-like morphology is more efficient in conversion than NPs. This enhanced efficiency may extend to other chemical reactions.

An ambient solution-state method for growing metallic brushes of micrometer length spread over cm^2 areas is presented. The brushes are composed of 1D assemblies of uniform nanoparticles, grown by the Coulombic forces present in the electrolytic spray system. Various control experiments prove that the electric field is the key to the oriented growth. The solvent

droplets are shown to deposit the metallic nanoparticle cargo one after the other, upon droplet collision at metallic surfaces. The growing brushes act as nanoscale antennae. The resulting structures are shown to act as molecular sensors due to their large surface enhanced Raman activity. Their porosity allows them to act as collector surfaces for particulate matter. Composition of such structures can be varied easily. Bimetallic Ag:Pd nanostructures act as catalysts for polymerization reactions. The ease of fabricating such structures directly from solutions and the efficient control of size and composition are expected to generate interest in this method for creating metallic grasslands.

Experimental Section

For all experiments, nanospray emitters were made using a micropipette puller (P-97) purchased from Sutter instrument, USA. MilliQ water was used for the electro spray experiments. A homemade nanospray source was made by pulling a borosilicate glass capillary (1.5 mm outer diameter and 0.86 mm inner diameter) using a micropipette puller and cutting into two pieces. The internal diameter of the spray tip was estimated to be 8–12 μm and electrode used was 0.5 mm diameter platinum wire (Sigma Aldrich, India). The capillary was filled with 1 mM aqueous solution of AgOAc using a micro-injector pipette tip. Experiments with different solvents mixtures (different composition of water/MeOH, water/acetonitrile, etc.) were also done. Water gave the best result among all the solvents, hence for all other experiments water was used as the solvent. The platinum wire was

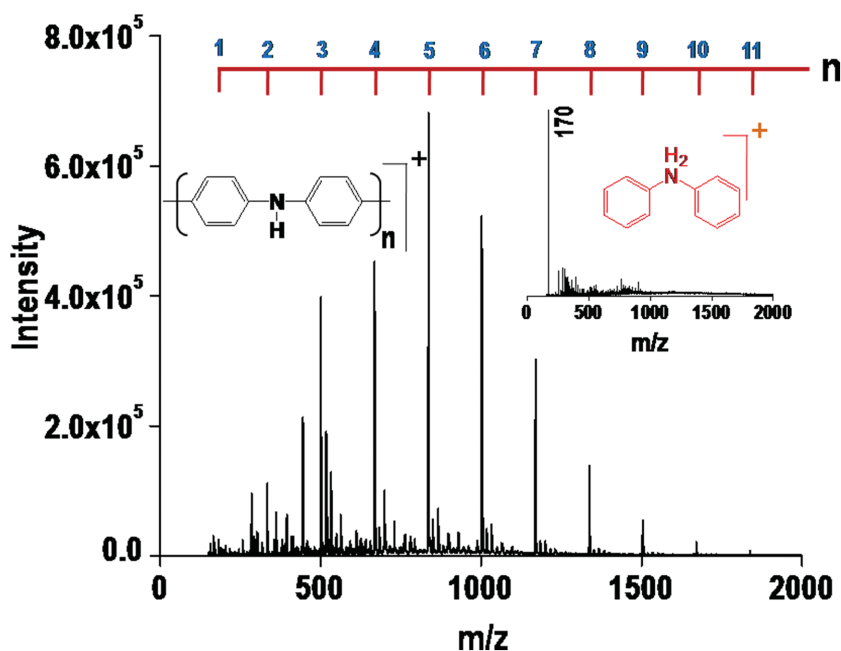


Figure 6. Mass spectrum taken after electro spray deposition of DPA on AgPd nanobrushes, showing polymerization of DPA. Inset shows the mass spectrum taken from electro spray deposited DPA on an ITO-coated glass slide.

connected to a high voltage power supply through a copper clip, and a potential in the range 1–1.5 kV was applied.

The collector surface, an ITO-coated glass slide in this case, was firmly mounted on a stable platform and a copper TEM grid was placed over it. The collector surface and the grid were grounded through a picoammeter. The spray emitter was manually positioned above the grid center at a distance of 5–10 mm and deposition was done. Parameters like distance of the spray emitter tip to the substrate and the deposition current, optimized by trial and error, were 5–10 mm and 20–40 nA, respectively. In the case of longer wires, we used 10 mm concentrations of aqueous silver salt (AgOAc). Electro spray of higher concentrations Ag gave similar structures in shorter time. From these images, it is clearly visible that the structures are not dendritic, they are 1D.

To confirm the presence of solvated Ag^+ ions, mass spectra were collected using an ion trap LTQ XL (Thermo Scientific, San Jose, California) mass spectrometer. Indium tin oxide-coated glass slides (Toshniwal brothers (SR) Pvt. Ltd., India) was the usual deposition substrate. Copper TEM grids with 100×100 micron apertures (Tedpella Inc. USA) were used as masks and served as substrates for NW growth. Locally available stainless steel wire mesh was used as substrate when indicated. All TEM measurements were made using a JEOL 3010 (JEOL Japan) transmission electron microscope. A field emission scanning electron microscope (FEI Quanta FEG 200, USA) was used to image these structures. EDS analyses were done with an attachment on the SEM instrument. Some images were collected with a FEI Quanta 100 instrument with tungsten filament source. Raman measurements were made using a Confocal Raman micro spectrometer (Witec GmbH, Germany) with 532 nm and 633 nm laser excitation. Silver acetate and palladium acetate (Sigma Aldrich, India) were used for electro spray. Hyperspectral images were collected with a Cytoviva instrument working in the spectral range of 400–1000 nm. XPS measurements were conducted using an Omicron ESCA probe spectrometer with polychromatic $\text{MgK}\alpha$ Xrays ($h\nu = 1253.6$ eV). Microparticles ($\text{PM}_{2.5}$) were generated by burning locally available incense sticks. *E. coli* were purchased commercially from MTCC (identification number MTCC 739).

Mechanical Stabilization of Ag Brushes: The brushes made of bare NPs have weak van der Waals interactions between the constituent NPs. Hence, they are not stable to mechanical strain. To increase stability to forces like the passage of air or immersion in water, postdeposition electro spray of 1,8-octanedithiol was done. It is expected that the terminal SH-groups will bind with two adjacent NPs and strengthen their bonding. Figure S11 in the Supporting Information shows SEM images of a dithiol-stabilized nanobrush on a TEM grid, before and after holding it under water. The image in Figure S11 B in the Supporting Information shows that brushes are lost from the grid due to the strain. Therefore, to bind the brushes to the substrate (TEM grid in this case), the 1,8-octanedithiol was electro sprayed on the substrate prior of creating the brushes. SEM images in Figure S11 C,D in the Supporting Information shows that nanostructures are now stable after water exposure.

Supporting Information

Supporting Information is available from the Wiley Online Library or from the author.

Acknowledgements

D.S., M.K.M. contributed equally to this work. The authors thank the Nano Mission, Department of Science and Technology, Govt. of India for continued support of our research program. D.S. thanks the

University Grants Commission and A.S. thanks Council of Scientific and Industrial Research for research fellowships. Financial support from the Separations and Analysis Program, Office of Basic Energy Sciences, US Department of Energy, DE-FG02-06ER15807 is also acknowledged.

Received: October 17, 2015

Revised: November 23, 2015

Published online: January 20, 2016

- [1] P. Christopher, S. Linic, *ChemCatChem* **2010**, *2*, 78.
- [2] a) M. A. Correa-Duarte, M. Grzelczak, V. Salgueirino-Maceira, M. Giersig, L. M. Liz-Marzan, M. Farle, K. Sieradzki, R. Diaz, *J. Phys. Chem. B* **2005**, *109*, 19060; b) S. Kralj, D. Makovec, *ACS Nano* **2015**, *9*, 9700.
- [3] Z. Tang, N. A. Kotov, M. Giersig, *Science* **2002**, *297*, 237.
- [4] a) X. Shen, L. Chen, D. Li, L. Zhu, H. Wang, C. Liu, Y. Wang, Q. Xiong, H. Chen, *ACS Nano* **2011**, *5*, 8426; b) H. Zhang, I. Hussain, M. Brust, M. F. Butler, S. P. Rannard, A. I. Cooper, *Nat. Mater.* **2005**, *4*, 787.
- [5] a) B. Freund, S. Suresh, *Thin Film Materials Stress, Defect Formation and Surface Evolution*, Cambridge University Press, Cambridge, United Kingdom **2003**; b) K. Wasa, M. Kitabatake, H. Adachi, *Thin Film Materials Technology: Sputtering of Compound Materials*, William Andrew Publishing, Norwich, New York **2004**; c) J. V. Barth, G. Costantini, K. Kern, *Nature* **2005**, *437*, 671; d) S. I. Stupp, V. LeBonheur, K. Walker, L. S. Li, K. E. Huggins, M. Keser, A. Amstutz, *Science* **1997**, *276*, 384; e) Y. Zhang, L. Zhang, C. Zhou, *Acc. Chem. Res.* **2013**, *46*, 2329; f) Y. Xia, P. Yang, Y. Sun, Y. Wu, B. Mayers, B. Gates, Y. Yin, F. Kim, H. Yan, *Adv. Mater.* **2003**, *15*, 353; g) G. Mondragon-Galicia, C. Gutierrez-Wing, M. Eufemia Fernandez-Garcia, D. Mendoza-Anaya, R. Perez-Hernandez, *RSC Adv.* **2015**, *5*, 42568; h) C. Chuang, S. Cheng, *Nano Res.* **2014**, *7*, 1592; i) S. H. Chung, S. Ramadurgam, C. Yang, *Nanomater. Nanotechnol.* **2014**, *4*, 58317/1; j) H.-W. Liang, J.-W. Liu, H.-S. Qian, S.-H. Yu, *Acc. Chem. Res.* **2013**, *46*, 1450; k) H.-W. Liang, S. Liu, J.-Y. Gong, S.-B. Wang, L. Wang, S.-H. Yu, *Adv. Mater.* **2009**, *21*, 1850; l) P. S. Chinthamanipeta, Q. Lou, D. A. Shipp, *ACS Nano* **2011**, *5*, 450.
- [6] a) G. L. Messing, S. C. Zhang, G. V. Jayanthi, *J. Am. Ceram. Soc.* **1993**, *76*, 2707; b) P. S. Patil, *Mater. Chem. Phys.* **1999**, *59*, 185.
- [7] a) N. Nasiri, R. Bo, F. Wang, L. Fu, A. Tricoli, *Adv. Mater.* **2015**, *27*, 4336; b) K. Okuyama, I. W. Lenggono, *Chem. Eng. Sci.* **2003**, *58*, 537; c) J. H. Bang, K. S. Suslick, *Adv. Mater.* **2010**, *22*, 1039.
- [8] R. Juraschek, T. Dulcks, M. Karas, *J. Am. Soc. Mass Spectrom.* **1999**, *10*, 300.
- [9] S. Parviainen, F. Djurabekova, A. Pohjonen, K. Nordlund, *Nucl. Instrum. Methods Phys. Res. Sect. B* **2011**, *269*, 1748.
- [10] E. T. Castellana, R. C. Gamez, M. E. Gomez, D. H. Russell, *Langmuir* **2010**, *26*, 6066.
- [11] a) S. Nie, S. R. Emory, *Science* **1997**, *275*, 1102; b) W. Deng, E. M. Goldys, *Analyst* **2014**, *139*, 5321; c) W. Xie, S. Schlucker, *Rep. Prog. Phys.* **2014**, *77*, 116502; d) P. El Khoury, G. E. Johnson, I. V. Novikova, Y. Gong, A. Joly, J. E. Evans, M. Zamkov, J. Laskin, W. Hess, *Faraday Discuss.* **2015**, *10.1039/C5FD00036j*; e) W. Hoffmann, G. Verbeck, *Appl. Spectrosc.* **2013**, *67*, 656.
- [12] C. Baker, A. Pradhan, L. Pakstis, D. J. Pochan, S. I. Shah, *J. Nanosci. Nanotechnol.* **2005**, *5*, 244.
- [13] C. Liu, P.-C. Hsu, H.-W. Lee, W. Li, M. Ye, G. Zheng, N. Liu, Y. Cui, *Nat. Commun.* **2015**, *6*, 6205.